The International Journal of Advanced Manufacturing Technology (2019) 100:1373–1382
https://doi.org/10.1007/s00170-018-2784-1

ORIGINAL ARTICLE

Improving deposition efficiency in cold spraying chromium coatings by powder annealing

Hwasung Yeom[1] · Tyler Dabney[1] · Greg Johnson[2] · Benjamin Maier[2] · Mia Lenling[2] · Kumar Sridharan[1,2]

Received: 5 July 2018 / Accepted: 25 September 2018 / Published online: 2 October 2018

Abstract

Annealing of attrition-milled, electrolytically produced chromium powder has been investigated to improve cold spray coating deposition efficiency of pure chromium on Zr-alloy substrate for light water reactors with the goal of enhancing high-temperature oxidation resistance. The annealing heat treatment at 800 °C for 5 h induced microstructural transitions in the powder such as the development of equiaxed grains and strain relaxation, both associated with a measured decrease in nano-hardness. Deposition efficiency of the annealed powder was about three times more than the as-received electrolytic Cr powder. In addition, the utilization of the annealed powder reduced substrate deformation effects. A qualitative explanation of the effects powder microstructure on the cold spray deposition process in terms of the resulting coating microstructures and deposition efficiencies has been introduced. Finally, high-temperature exposure tests indicated that oxidation resistance of these Cr coatings was comparable to that previously reported for those produced using gas-atomized Cr powder. This study suggests that annealing of electrolytic Cr powder is a practical and economically favorable pathway to produce oxidation-resistant cold spray Cr coatings. More generally, use of the widely available electrolytic and mechanically milled powder vastly opens scope of cold spray deposition process, where atomized powders may not be either available or challenging to produce.

Keywords Cold spray process · Electrolytic Cr powder · Powder annealing · Deposition efficiency · Oxidation resistance

1 Introduction

Chromium coatings have been used for decorative and functional purposes in a wide range of industrial applications that include automotive, aerospace, energy, and manufacturing industries. Traditional chromium coatings have been prepared by commercial electroplating techniques which show excellent properties including resistance to wear and corrosion, a low friction coefficient, high hardness, and lustrous surface appearance [1]. Recently, the development of thin chromium (Cr) coatings for the zirconium-alloy fuel cladding material in light water reactors (LWRs) has drawn considerable attention in nuclear industries and research institutions. Cr has been investigated as coating material for accident-tolerant fuel cladding by improving high-temperature air and steam oxidation resistance in accident conditions without significant modifications of the current LWR design. Given the critical requirements for the nuclear reactor application, several methods have been investigated to deposit Cr coatings on Zr-alloys [2–6].

One promising coating technology for depositing Cr on Zr-alloys for LWR fuel cladding with demonstrated success is the cold spray process [6, 7]. In the cold spray process, microns-sized feedstock powder is propelled at supersonic velocities (Mach 2–3) on to the surface of a substrate using pressurized gas flowing through a converging/diverging nozzle system. The particle temperature is low and the deposition occurs in solid state. Above a certain particle velocity (i.e., critical velocity), a dense and adherent coating/deposit can potentially form on the substrate due to high-strain-rate plastic deformation of particles and an associated adiabatic shear mechanism [8]. Since the particle temperature is low and the particles have a very short residence time in the carrier gas stream, the deposits are relatively free of secondary phases and oxide inclusions, and are strongly adhered to the substrate [9]. However, thermal spray process involves melting of powder feed by a

✉ Kumar Sridharan
kumar.sridharan@wisc.edu

[1] Department of Engineering Physics, University of Wisconsin-Madison, 1500 Engineering Drive Rm, Madison, WI 53706, USA

[2] Department of Materials Science & Engineering, University of Wisconsin-Madison, Madison, WI 53706, USA

concentrated heat source (e.g., plasma and combustion) followed by solidification of deposited material, potentially leading to oxidation of the powder, and the presence of oxide inclusions in the coatings, porosity, and phase segregation in the coatings [10]. The cold spray process is performed at atmospheric pressure with a high deposition rate, which makes it commercially attractive for the manufacture of the full-length of Cr-coated fuel claddings. Our previous work demonstrated the development of cold spray process using a spherical Cr powder (manufactured by gas atomization process) for Zr-alloy tubes with a length of ~ 300 mm to produce high-density coatings, approximately 100 μm in thickness [6, 11, 12]. Excellent oxidation resistance of the coatings was confirmed even at 1300 °C in both ambient air and steam environments. After steam oxidation tests, the coated samples retained more ductility due to the decreased hydriding and oxidation of the underlying Zr-alloy cladding. Moreover, adhesion strength between the Cr coatings and the Zr-alloys substrate was strong as evidenced by absence of any spallation or delamination of the coatings even up to the point of failure of the coated cladding tubes in tensile tests.

Deposition efficiency of the cold spray process strongly depends on intrinsic characteristics of the feedstock powder such as its morphology and mechanical properties which dictate its deformation behavior. The thickness and properties of the oxide films present on the powder particles' surface will also have a profound effect on the deposition efficiency as the coating formation relies on the high-strain and high-strain-rate plastic deformation of the particles upon impact to create the metallurgical bonding and mechanical interlocking [13]. For example, Assadi et al. [8] proposed that deposition efficiency is inversely proportional to the melting point and the ultimate tensile strength of particles, but directly proportional to the density of the feedstock powder. If impinging particles have limited deformability, they either bounce of the substrate or erode its surface instead of depositing. Therefore, functional ceramics or some hard alloys must be sprayed as composites in combination with relatively softer metals or alloys which increases the overall deformability of the coating powder mixture (e.g., SiC-Al [14], Cr_3C_2-NiCr [15, 16], and CoCr-316 L stainless steel [17]). It is worth noting that pure chromium exhibits little or no tensile ductility at room temperature [18], has a high melting point (i.e., 1875 °C [19]), and a high hardness. Thus, it may be expected that its deposition efficiency would be lower than softer metal powders such as aluminum and copper where thick coatings in thickness of tens of millimeter have been reported [20]). Therefore, in our previous studies, optimization of the cold spray process for Cr was rigorously performed to achieve 100 μm coating thicknesses using a gas-atomized powder [6, 21]. The gas-atomized powder had a spherical morphology and a reasonable capacity for plastic deformation due to its relative softness. However, gas-atomization processing for fine Cr powder is challenging due to its high melting point and reactivity, and environmental and safety concerns due to potential formation of toxic gaseous Cr(VI) compounds, resulting in a high production cost. An alternative powder form is electrolytic powder, manufactured from mechanical attrition and refinement of electrolytic Cr flakes or plates. The cold spray process using electrolytic Cr powder could improve cost effectiveness compared to atomized Cr powder, but the deposition efficiency is likely degraded due to its inherent residual stresses and deformation introduced from the mechanical attrition process.

In the present study, the cold spray process using electrolytic Cr powder for Zr-alloy substrates was investigated as an alternative for Cr coating using gas-atomized Cr powder. An annealing process for the as-received electrolytic Cr powder and cold spray parameters were investigated to achieve a high-quality coating with respect to coating thickness and microstructure. The coated samples were evaluated for oxidation resistance by exposure of the samples at 1200 °C for 20 min in ambient air. The experimental results may suggest a potential pathway for cost-effective, cold spray-coated Cr using a commercial electrolytic Cr powder while maintaining its performance. The study also puts forward a better understanding of the particle/particle and particle/substrate interactions during the cold spray process.

2 Experimental

Commercially, pure electrolytically produced Cr powder (99.8% purity) below 44 μm (− 325 mesh) was procured from Atlantic Equipment Engineers (Upper Saddle River, NJ USA). The Cr powder was mechanically sieved to retain particles below 25 μm. The sieved powder is referred to as the as-received powder in this study. Zr-alloy plates with thicknesses of 2.8 mm (Zircaloy-4 grade: 0.18 wt% Fe, 0.09 wt%O, 0.07 wt%Cr, and balance Zr) was used as the substrate material and was procured from ATI Wah Chang (Albany, OR, USA). The plates were sectioned to dimensions of 25 mm × 25 mm, ground with 320 grit SiC abrasive paper, and thoroughly cleaned using distilled water and then ethanol multiple times. Any trace surface impurities are likely to be removed due to ablation by the high-velocity impinging particles.

Heat treatment for the as-received Cr powder was performed at a commercial heat-treating company (Solar Atmospheres, Souderton PA, USA) with the intent of decreasing hardness and increasing deformability. The annealing was conducted at 800 °C for 5 h in an argon environment along with pure titanium sponge to minimize residual oxygen in the annealing environment. Some particle agglomerates formed during this heat treatment but readily disintegrated to separate powders during mechanical sieving. Both the as-received and the annealed powders were used for cold spraying.

A commercial Cold Gas Technologies Kinetiks 4000/34 unit system was utilized for deposition of the as-received and the annealed Cr powders. The cold spray system consists of a Type 24 tungsten carbide nozzle (converging-diverging De Laval nozzle), a powder feeder, a gas pre-heater, and a six-axis robot arm to control the position of the spray nozzle. Coatings were deposited using both industrial grade nitrogen and mixtures of nitrogen and helium as the propelling gas. The Zr-alloy flats were held normal to the spray gun. Standoff distance (26 mm), gas pressure (4.0 MPa), and powder feed rate (2 rpm) were held constant while other parameters (i.e., composition and temperature of working gas) were varied to study their effects on the characteristics of the cold spray coating. Helium gas was mixed with nitrogen gas to increase velocity of the Cr particles. The propellant gas pre-heat temperature which provides additional driving force for particle propulsion was maintained as high as the heating system would allow for a given gas mixture composition. Table 1 summarizes the cold spray deposition process parameters used in this study.

Nano-hardness values for the Cr powders was obtained using a standard Berkovich diamond tip driven into and withdrawn from cross-sections of Cr particles using a Hysitron Ti-950 Triboindenter system. Maximum displacements were 175 nm and the tests were conducted at room temperature. As a preliminary test to assess the efficacy of Cr coating produced from annealed powder for high-temperature oxidation resistance, exposure tests of the Cr-coated Zr-alloy were performed in ambient air. The coated samples were loaded into a pre-heated alumina tube furnace (Model GSL1600X) at a temperature of 1200 °C for 20 min in ambient air. After the exposure, the samples were rapidly air-cooled to room temperature. The rapid heating and cooling thermal profile provided qualitative assessments of the thermal shock resistance of the coating-substrate system.

Powder morphology and cross-sectional microstructure of the coatings were characterized by a Zeiss LEO scanning electron microscopy (SEM) in conjunction with x-ray energy dispersive spectroscopy (EDS). Cross-sectioned feedstock powders and as-deposited coatings were etched with the Murakami reagent (10 g NaOH, 10 g Potassium Ferricyanide ($K_3Fe(CN)_6$), 100 mL DI water) for 30 s at room temperature to reveal the microstructure more clearly. Phase identification of the powders and coatings was performed using Bruker D8 Discovery X-ray diffraction (XRD) with Cu Kα radiation (wavelength 1.5405 Å) and diffracted beams were acquired from 30° to 90° with coupled 2θ mode. The grain sizes of Cr powders were measured at four evenly spaced directions (0°, 45°, 90°, 135°) of each grain in cross-sectional SEM images and averaged as per ASTM E1382 [22]. Coating thickness and interfacial roughness (i.e., a peak-to-valley distance of substrate-coating interface) between the Cr coating and the Zr-alloy substrate were quantified for each spray condition using multiple SEM images and image post-processing software (ImageJ, Ver. 1.5b).

3 Results and discussions

3.1 Electrolytic Cr powder and coating characterization

Figure 1 shows SEM micrographs of the as-received Cr powder after mechanical sieving. The plan-view SEM image (Fig. 1a) reveals irregular and jagged particles that are less than 25 μm in size. The cross-sectional image of the interior of the particles as examined by SEM (Fig. 1b) showed minor cracks with very fine, submicron grains are shown. Analysis of the as-received feedstock powder particles showed the average nano-hardness value to be 6.7 ± 0.7 GPa which is higher than nano-hardness of polycrystalline bulk Cr (2.3 GPa) [23]) and single crystalline bulk Cr (1.6 GPa [24]) reported in literature. It is speculated that the high hardness value results from the cold-working induced during manufacture of the powder and the inherently fine grain size of electrolytic Cr. For example, fine-grained Cr produced by means of high-pressure torsion showed approximately three times higher nano-hardness value than that of single crystal bulk Cr [24].

The as-received Cr powder was deposited on Zr-alloy flats for different spray conditions and the cross-sectional SEM images of the coatings are shown in Fig. 2. All spray conditions produced continuous Cr coatings on the substrate and no spallation of the coatings from the substrate was observed. However, deposition efficiency (i.e., coating thickness) was not significantly improved by the helium carrier gas conditions (Spray#2 and Spray#3). Instead, horizontal cracks were identified in the coatings as shown in Fig. 2b, c. It is known that quality of the cold spray coatings tends to improve with helium propellant gas due to a higher velocity of powder, resulting in higher density and thicker coatings. This trend

Table 1 Variables of the cold spray process for the deposition of Cr coatings. A ratio of the gas flow rate of nitrogen to helium is specified in the parenthesis (N_2:He) if the gas mixture was used. The annealed powder was heat treated at 800 °C for 5 h in an inert gas environment

Spray condition	Composition of working gas (N_2:He)	Gas preheat temperature	Feedstock powder
Spray #1	Pure N_2	750 °C	As-received powder or annealed powder
Spray #2	N_2 + He (25%:75%)	550 °C	As-received powder or annealed powder
Spray #3	N_2 + He (5%:95%)	500 °C	As-received powder or annealed powder

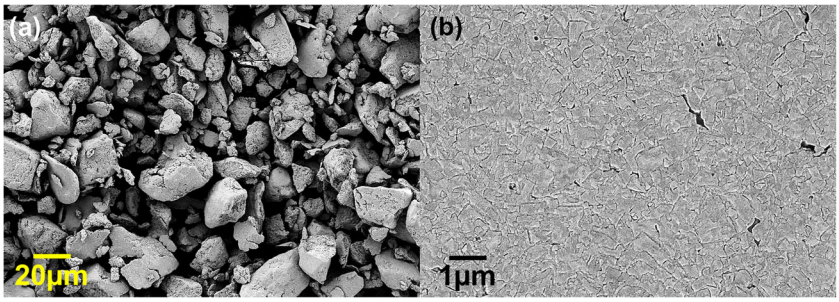

Fig. 1 **a** Plan-view SEM image of as-received electrolytic powder after sieving < 25 μm and **b** high-magnification cross-sectional SEM image of individual powder particle. A low accelerating voltage (3 kV) was used in the SEM for better resolution imaging. The cross-section of the powder particle was etched with Murakami reagent to reveal the microstructure

for Cr deposition was reported in previous work by the authors [21], where thick Cr coatings (~ 100 μm) were produced on Zr-alloy using gas-atomized Cr powder and helium carrier gas. It is believed that this difference is related to the high hardness and limited deformability of the as-received powder as will be discussed further in a later section. In addition, the etched Cr coating (Fig. 2d) exhibited the fine grains with some cracks. General particle impact boundaries inherent to cold spray deposited coatings showing bands of elongated and refined grains [25, 26] were not identified clearly in the SEM images of the present coatings. This suggests that the mechanisms of particle-to-particle bonding may be different from softer powders reported in cold spray literature and our own studies with atomized Cr powders [6]. In addition, it was confirmed by XRD that no phase changes or oxidation of the feedstock powder occurred during the cold spray deposition processes.

3.2 Annealed Cr powder and coating characterization

Annealing for the as-received electrolytic Cr powder was performed at 800 °C for 5 h to improve the microstructure of the feedstock powder for cold spray deposition. The annealing was performed under argon atmosphere and with titanium sponge both to reduce oxidation of the chromium powder which may interfere with coating formation in cold spray process. The irregular powder morphology was maintained during the annealing process, suggesting that particle velocity for the annealed powder would be identical to the as-received powder under the same cold spray process condition. Figure 3 shows higher magnification micrographs of the as-received and the annealed Cr powder, respectively. As indicated earlier, the as-received powders exhibit fine grains and needle-shaped pores between the grains (Fig. 3a) while annealing of the powder at 800 °C led to the evolution of the microstructure to larger, well-defined, and equiaxed grains as shown in Fig. 3b. It was anticipated that larger grain size contributes to improve the deformation capability of the powder which can promote higher deposition efficiency. The annealing also reveals second phase particles, likely oxides distributed sporadically in the microstructure. The nano-scaled particulates (less than 90 nm) were mainly identified at the grain boundaries. The surface of the annealed powder (Fig. 3d) also exhibited a higher number density of the particulates than that on the cross-sections of particles. However, there was no evidence of a continuous oxide layer on the surface

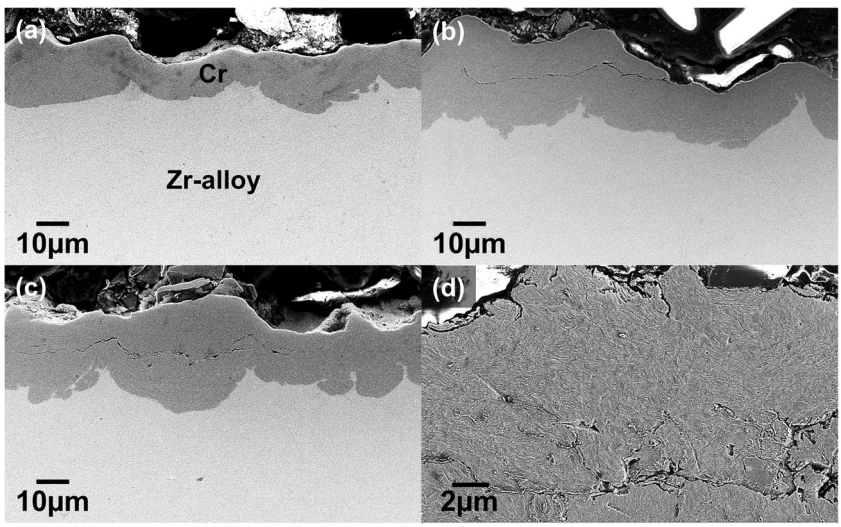

Fig. 2 Cross-sectional SEM images of Cr coatings on Zr-alloy flats with different spray conditions using as-received electrolytic Cr powder. **a** Spray #1, **b** spray #2, and **c** spray #3 (please see Table 1). The images were acquired using 10 kV accelerating voltage for better compositional contrast. Some cracks in the coating produced by spray #1 condition after etching are shown in (**d**) which represent higher magnification image taken at 3 kV accelerating voltage

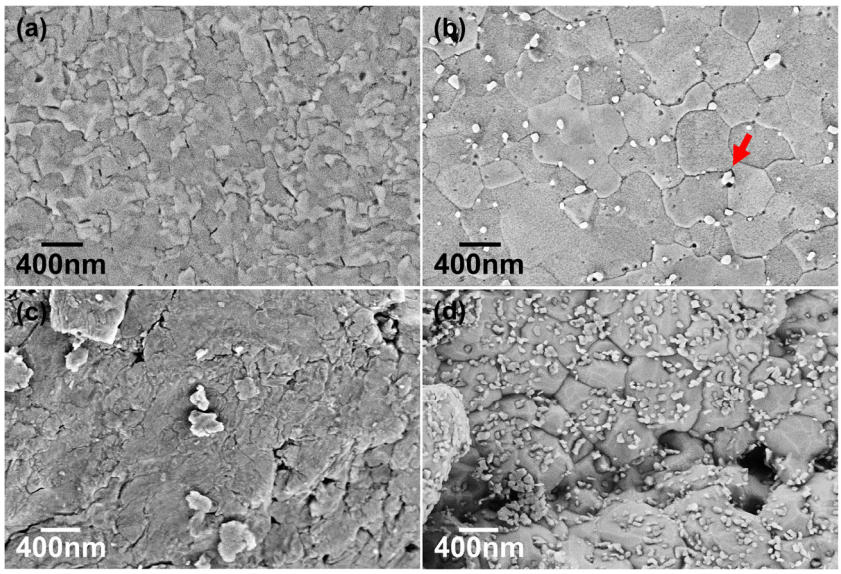

Fig. 3 Cross-sectional SEM images of **a** as-received Cr powder and **b** annealed Cr powder (etched with Murakami reagent). The images were taken using 3 kV accelerating voltage. The red arrow indicates nano-sized particulate which is likely oxide. Plan-view SEM images of **c** as-received Cr powder and **d** annealed Cr powder. The outer surface of annealed Cr powder showing discrete nanoparticles of oxide rather than a continuous oxide layer

which may impede interparticle cohesion or particle-substrate adhesion. The imaging contrast between the grain background matrix and particulates suggests differences in their compositions. It is speculated that the surface oxide particulates formed by the reaction with residual oxygen in the controlled environment. Unfortunately, the size of the particulates was too small to be characterized with respect to the composition by SEM-EDS analysis. Furthermore, XRD analysis did not provide any diffracted peaks emanating from a second phase due to the small volume fraction of these particulates in the powder as shown in Fig. 5a.

The grain size and nano-hardness values for the as-received powder and the annealed powder are plotted in Fig. 4. After the heat treatment at 800 °C, the grain size increased from 328 ± 113 to 586 ± 121 nm. The nano-hardness value decreased from 6.7 ± 0.7 to 4.2 ± 0.5 GPa. The annealing process induced recovery and recrystallization of the cold-worked Cr powder which led to relief of local strain and grain growth.

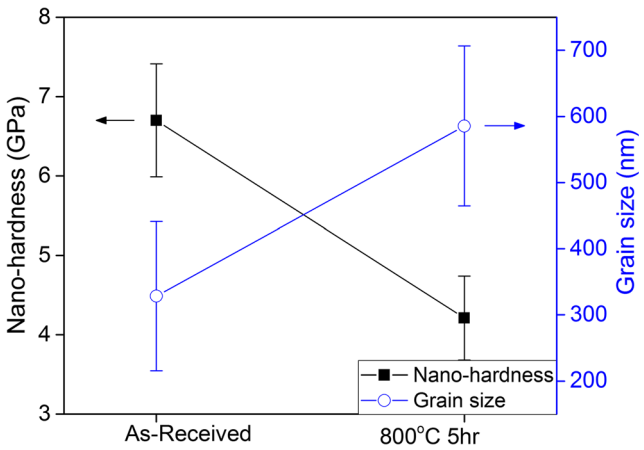

Fig. 4 Nano-hardness and measured grain size of as-received Cr powder and annealed Cr powder

The softening of the as-received powder was attributed to the decrease in dislocation density and the grain growth (i.e., the latter dictated by Hall-Petch relation [27]). A significant hardness drop was also reported for annealing of cold rolled Cr plates (78 to 91% reduction) in the range of 800 to 1000 °C [18] and the Hall-Petch relationship has been shown to hold good in literature for electrodeposited Cr in grain diameter of 0.1 to 10 μm [28].

The XRD patterns of the as-received Cr powder, the annealed powder, and the as-sprayed coating formed using the heat-treated powder by Spray #3 condition are shown in Fig. 5a. Identical x-ray peaks are observed corresponding to pure body-centered cubic (BCC) chromium with no additional distinguishable peaks, indicating that the phase purity of the feedstock materials was preserved during the powder deposition process without large-scale oxide phase formation. In addition, noticeable peak sharpening/broadening was observed during the series of powder annealing and cold spray processing. Figure 5b shows (110) reflection peaks of the as-received powder, the annealed powder, and the as-sprayed coating using the annealed powder. The diffraction peak for the as-received powder becomes sharper after the annealing, and as-sprayed coating shows peak broadening. It is experimentally known that the width change of the x-ray diffraction peaks arises from a combination of grain refinement/coarsening and local strain in the matrix [29, 30]. Hence, it can be concluded that the peak sharpening between the as-received and annealed powder resulted from the strain relaxation and recrystallization during the heat treatment and the peak broadening between the annealed powder and coating was induced by the work hardening associated with the severe plastic deformation of the powder particles during the coating formation.

A selection of as-sprayed coating microstructures of the Cr coatings formed using the annealed Cr feedstock powder is

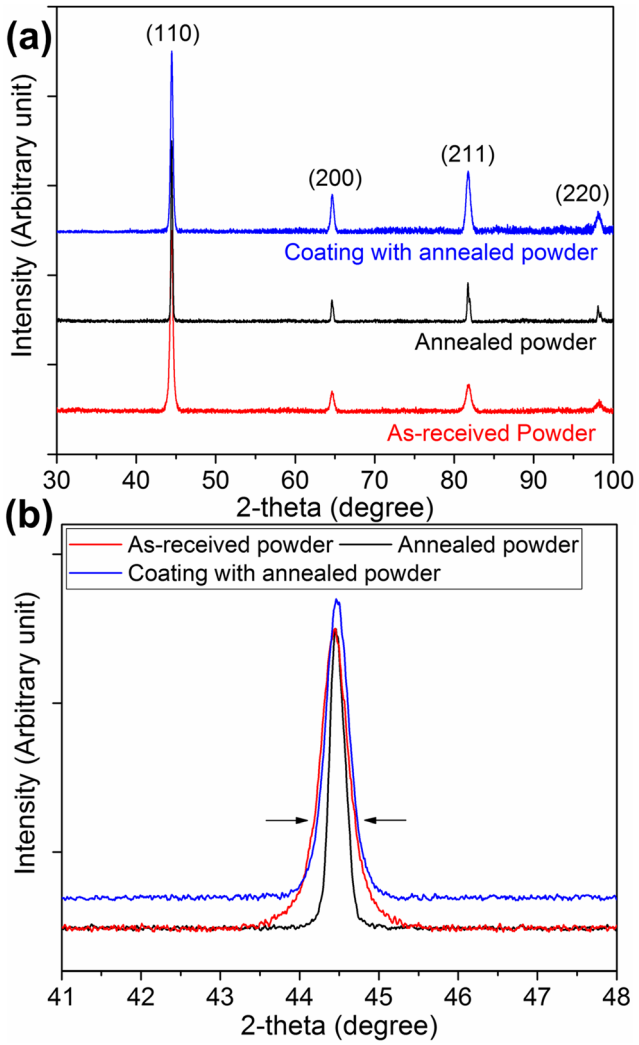

Fig. 5 **a** X-ray diffraction patterns of the as-received Cr powder, the annealed powder, and coating produced using the annealed powder using spray #3 conditions. **b** A close-up view of the (110) peaks for as-received powder, annealed powder, and coatings deposited by annealed powder to emphasize the differences in peak widths after each processing method

shown in Fig. 6. As can be seen from these images, deposition of thick, dense, and continuous Cr coatings on Zr-alloy substrate was successfully achieved using the annealed Cr powder. The presence of oxide nano-particulates in the annealed powder did not seem to have any significant effect on coating build-up or its quality in regard to spallation or cracking. Regardless of the spray conditions, the coatings produced by annealed powders were two or three times thicker than those produced using the as-received Cr powder. Spraying with addition of helium to the propellant gas mixture resulted in higher deposition efficiency (i.e., thicker coating), providing room for post-surface processing to decrease surface roughness without a coating breach. It is important to note that bands of deformed grains were seen in certain areas of the coatings as shown in Fig. 6d. Moving further away from the band, a coarser-grained microstructure was observed, similar to that of the unsprayed, annealed powder particles. It is believed that these bands of extensive deformation are localized to the particle-particle interfaces in the coating. The high-velocity particle impact on coating surface led to intense deformation at the contact interfaces, resulting in elongation of the grains near the particle-particle interface, but the interior of the particle remained relatively undeformed. Similar heterogeneous microstructures of cold-sprayed coatings were also observed in other studies [25, 31].

3.3 Coating thickness and interfacial roughness

The cold spray processes using the as-received powder and the annealed powder resulted in continuous and high-density coatings (with negligible porosity) on the substrate. The dependence of the measured coating thicknesses and peak-to-valley distances of the interface between the coating and the substrate on the feedstock powder and spray condition is summarized in Fig. 7. Coating thicknesses using the annealed powder were increased from 32 to 63 μm with increasing helium content in the carrier gas. This is a significant improvement over coatings made with the as-received chromium powder. These coatings were about 20 to 40 μm thinner than those produced with the annealed powder. The maximum coating thickness for the case of as-received powder was only 23 μm in the highest particle velocity (spray #3). In addition, interfacial roughness for the coatings deposited with the annealed powder did not vary significantly with respect to the spray conditions. The as-received powder produced coatings where the interface roughness increased with helium content. It is true that some interfacial roughness is required for strong adhesion between the coating and the substrate; however, rough interfaces also lead to non-uniformity in coating thickness and must be controlled. The as-received powder tended to erode and deform the substrate and the effect was more pronounced with increasing in-flight velocity of the particles (i.e., higher helium content). The softened and resulting enhanced deformability of the annealed powder facilitated easier plastic deformation of these particles upon impact, maintaining a similar degree of substrate damage (e.g., extrusion and erosion) regardless of the spray conditions.

3.4 Oxidation resistance at high temperature

High-temperature exposure tests at 1200 °C for 20 min in ambient air were conducted to evaluate oxidation resistance of the Cr coatings produced with the annealed powders. The coatings were polished using 600 grit SiC abrasive paper to remove the surface roughness prior to the high-temperature test. Cross-sectional SEM images of the Cr coating after the oxidation test are shown in Fig. 8a. A thin chromium oxide layer (4~5 μm) was observed on top of the Cr coating,

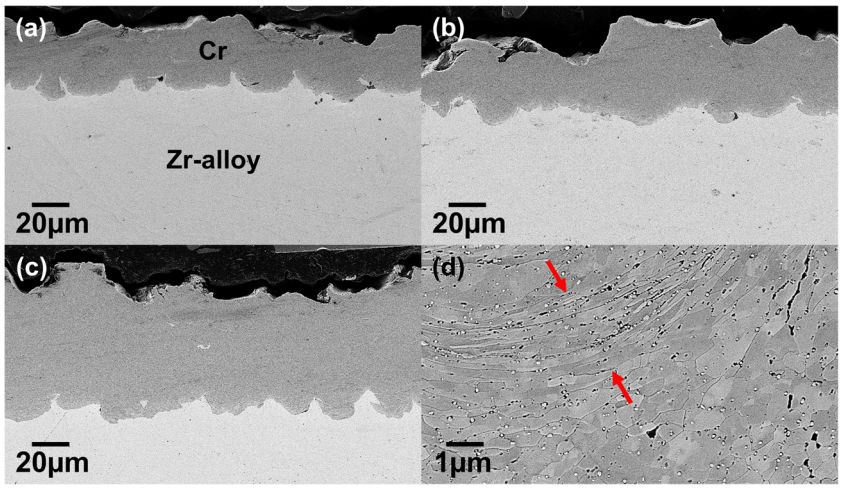

Fig. 6 Cross-sectional SEM images of as-sprayed Cr coatings on Zr-alloy substrates using annealed Cr powder with different spray conditions: **a** spray #1, **b** spray #2, and **c** spray #3. The images were taken using 10 kV accelerating voltage and the magnification is different from Fig. 2. **d** Higher magnification image (3 kV accelerating voltage) of (**b**) after surface etching. The red arrows indicate a band of heavily deformed grains in a localized area of the coating

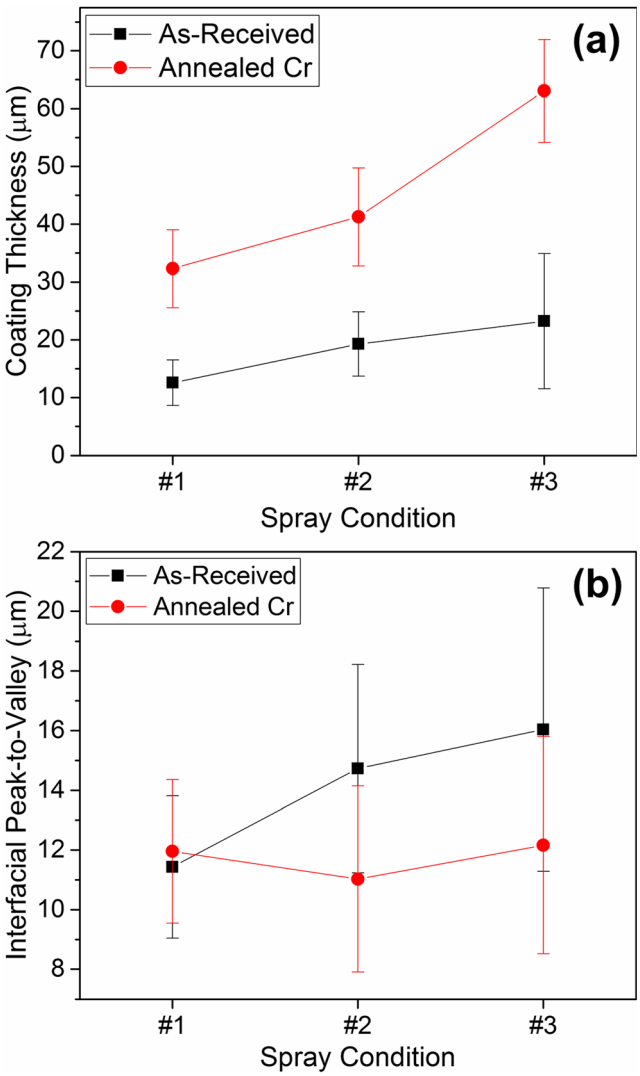

Fig. 7 **a** Cr coating thickness and **b** interfacial roughness (a peak-to-valley distance) between Cr coatings and Zr-alloy substrate as a function of feedstock powder and spray condition

inhibiting further oxidation of the coating and protecting of the underlying Zr-alloy substrate. In comparison, a thick zirconium oxide scale (~ 92 μm) developed on the uncoated side of the substrate (Fig. 8b). This result is consistent with oxidation tests of Cr coatings deposited using atomized Cr powder on Zr substrates [6], suggesting that the use of annealed electrolytic Cr powder rather than the gas-atomized Cr powder may be a promising alternative.

3.5 Cold spray deposition mechanism of as-received powder and annealed powder

Based on the experimental results, a hypothetical model is proposed for the evolution of the coating microstructure during cold spray deposition of the as-received and the annealed electrolytic powders. Schematic illustrations of the microstructural evolution of the particle-to-substrate and particle-to-particle interfaces for each of the two types of powders are shown in Fig. 9. An as-received particle impacts the substrate and the substrate experiences microscopic extrusion at the contact interface due to the limited deformation of the hard particle impact, as shown in Fig. 9a, b. Plastic deformation of the particle upon impact is localized to the colliding particle's surface. As successive particles impact the coating surface, some of the impinging particles adhere to the existing coating if the colliding surfaces are aligned such that they slide against one another to form a frictional bond. A larger fraction of the impinging particles rebound as the colliding surfaces are not aligned to facilitate this weak mechanical interlocking, resulting in the low deposition efficiency. In other words, if certain faces of the Cr particles are not aligned correctly, they will not cohere; however, if they are aligned properly such as teeth of one wheel locking into the teeth of another, they can lock together and form a coating, as illustrated in Fig. 9c. The cohesion between these hard Cr particles is thus mainly attributed to frictional interlocking and shearing/sliding process

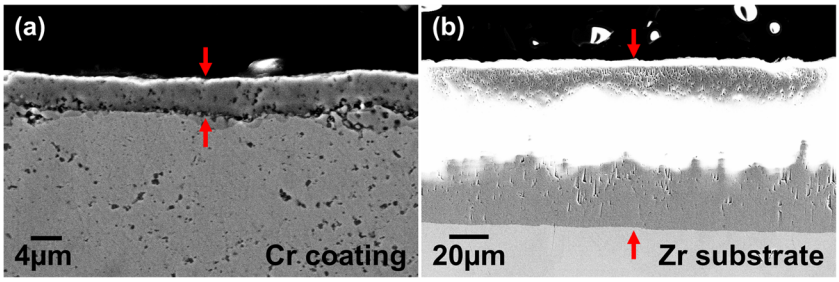

Fig. 8 Cross-sectional SEM images of Cr coating deposited using annealed powder on the Zr-alloy substrate after exposure at 1200 °C for 20 min in ambient air: **a** a high-magnification image showing a thin oxide layer (~4.5 μm) on the Cr coating and **b** a low-magnification image revealing a thick oxide layer (~92 μm) on the uncoated surface of the Zr-alloy (the brightness of the image is due to electron charging effects stemming from the insulating nature of the oxide layer). The annealed powder was sprayed with spray #3 condition and then polished using 600 grit SiC abrasive paper prior to the oxidation test. The images were acquired with 10 kV accelerating voltage for enhanced compositional contrast. The red arrows indicate the oxide layers

during impact. The minimal plastic deformation of the particles also leaves cracks or pores between the interparticle boundaries as shown in Fig. 2d.

In comparison to the as-received powder particle, when an annealed powder impacts the substrate, a larger portion of the impact energy is converted to the plastic deformation of the particle with less energy consumed by substrate deformation, as illustrated in Fig. 9d, e. The plastic deformation occurs over the colliding interface with the associated adiabatic instability in this case providing a larger contact area for strong interfacial interlocking and metallurgical bonding [8], resulting in a larger fraction of the impinging particles successfully depositing as shown in Fig. 9f. The higher capacity for particle deformation is attributed to the larger grain size and lack of strain hardening, as observed in Figs. 3 and 5, so that initiation of plastic deformation and dislocation nucleation and movement become relatively easier. It is known that deposition efficiency in the cold spray process tends to increase with decreasing yield strength of the feedstock material [8] and the flow stress of work-hardened material is proportional to its hardness [32]. Therefore, the coating thickness of a soft powder (e.g., the annealed powder) can be higher than that of a hard powder (e.g., the as-received powder).

3.6 Effect of impurity in powder on cold spray process

A thick cold spray coating using the annealed powder was successfully achieved even though the annealed powder contained nano-sized second phases (70 to 90 nm) dispersed at the grain boundaries and powder surfaces as shown in Fig. 3b, d. It appears that the deformation of the powder particles upon impact was not significantly influenced by the nano-particulates at the grain boundaries. Oxide-free and clean interfaces between particle and substrate or adjacent particles are required to attain metallurgical bonding in cold spray coatings. It is hypothesized that the impurities on the particle surfaces were disrupted and cleaned out as the particles impacted the substrate due to the severe and rapid plastic deformation. For instance, Chen et al. [33] reported experimental evidence of this

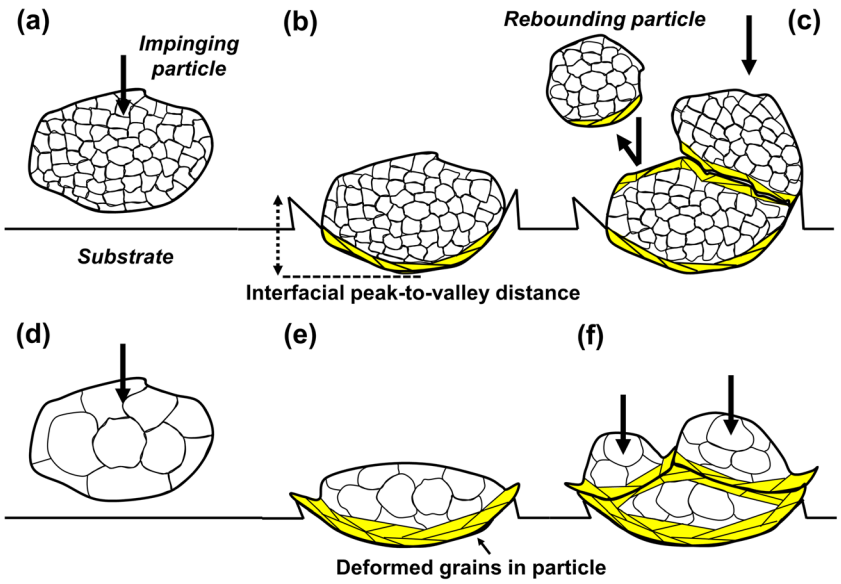

Fig. 9 Schematic illustration of the evolution of microstructure in cold-sprayed coatings of (**a**–**c**) as-received electrolytic powder and (**d**–**f**) annealed electrolytic powder and the deformation of the underlying substrate. The deformed area containing the elongated grains is highlighted by the yellow color

cleaning effect by extrusion of viscous metal jets of oxidized Cu particles in the cold spray process, where oxide fragments were only identified at the periphery of the deposited particle and a clean contact area was observed between the central area of the particle and substrate. Also, Li et al. [34] showed an increase in oxygen content of Ti cold spray coatings compared to the feedstock powder if compressed air was used as a carrier gas. Yet, high deposition efficiency and metallurgical bonding between the Ti particles were still observed, so that the authors proposed a strong friction effect between particles inducing break-up of oxide films on the Ti particles.

4 Conclusion

The present study demonstrated the improvement of the deposition efficiency in cold spray process of electrolytic chromium powder on Zr-alloy substrate which can be achieved by annealing of the feedstock powder. The annealing was performed at 800 °C for 5 h in the argon environment in order to increase deformation capability of the powder particles. The environmental condition for annealing was maintained inert enough so as to not induce the formation of a continuous oxide layer on the particle surface which may impede coating formation and adhesion. Microstructural evolution of the powder after the annealing and the microstructure of the as-sprayed coatings deposited using various spray parameters were characterized and analyzed. After the annealing, the electrolytic powder exhibited well-defined and equiaxed grains, and grain growth from ~328 to ~586 nm. XRD patterns showed peak sharpening of bcc chromium peaks due to the annealing, which is indicative of strain relaxation as well as grain coarsening. Moreover, nano-hardness values of the powder particles decreased from 6.7 to 4.2 GPa as a result of the annealing treatment. The cold spray process using the annealed powder improved deposition efficiency significantly (up to 270%) and reduced substrate deformation. Heavily deformed grains were identified in local areas of the coatings, which were not clearly observed in the coatings with the as-received electrolytic powder. A qualitative explanation for the microstructural evolution and the improved deposition efficiency for the annealed powder has been proposed based on experimental observations. Finally, the Cr cold spray coatings showed excellent oxidation resistance when tested at 1200 °C in ambient air. The results of this study suggest that annealing of commercial electrolytic Cr powder is a practical pathway for a cost-effective cold spray Cr coating while maintaining its performance as an alternative to using gas-atomized Cr powder. By demonstrating that powder annealing can increase deposition efficiency, the study opens the scope of the cold spray process for the effective deposition of a larger range of coating materials, for which powders may not be available in atomized form.

Acknowledgements The authors wish to acknowledge the support from Westinghouse Electric Company. The authors also thank Solar Atmospheres, Inc., Souderton, PA (Dr. Virginia Osterman) for performing the annealing of the chromium powders. This work is sponsored by the US Department of Energy, Office of Nuclear Energy, under grant number DE-NE0008222.

References

1. Almotairi A, Warkentin A, Farhat Z (2016) Mechanical damage of hard chromium coatings on 416 stainless steel. Eng Fail Anal 66: 130–140. https://doi.org/10.1016/j.engfailanal.2016.04.011
2. Kim HG, Kim IH, Il JY et al (2015) Adhesion property and high-temperature oxidation behavior of Cr-coated Zircaloy-4 cladding tube prepared by 3D laser coating. J Nucl Mater 465:531–539. https://doi.org/10.1016/j.jnucmat.2015.06.030
3. Wang Y, Zhou W, Wen Q, Ruan X, Luo F, Bai G, Qing Y, Zhu D, Huang Z, Zhang Y, Liu T, Li R (2018) Behavior of plasma sprayed Cr coatings and FeCrAl coatings on Zr fuel cladding under loss-of-coolant accident conditions. Surf Coat Technol 344:141–148. https://doi.org/10.1016/j.surfcoat.2018.03.016
4. Arnal BB (2018) Atomic-scale interface structure of a Cr-coated Zircaloy-4 material. J Mater Sci 53:9879–9895. https://doi.org/10.1007/s10853-018-2333-1
5. Park DJ, Kim HG, Il JY et al (2016) Behavior of an improved Zr fuel cladding with oxidation resistant coating under loss-of-coolant accident conditions. J Nucl Mater 482:75–82. https://doi.org/10.1016/j.jnucmat.2016.10.021
6. Maier B, Yeom H, Johnson G, Dabney T, Walters J, Romero J, Shah H, Xu P, Sridharan K (2018) Development of cold spray coatings for accident-tolerant fuel cladding in light water reactors. JOM 70: 198–202. https://doi.org/10.1007/s11837-017-2643-9
7. Lahoda E, Xu P, Karoutas Z, et al (2018) Cold spray chromium coating for nuclear fuel rods. US Patent:US 2018 / 0025793 A1
8. Assadi H, Gärtner F, Stoltenhoff T, Kreye H (2003) Bonding mechanism in cold gas spraying. Acta Mater 51:4379–4394. https://doi.org/10.1016/S1359-6454(03)00274-X
9. Ajdelsztajn L, Jodoin B, Kim GE, Schoenung JM (2005) Cold spray deposition of nanocrystalline aluminum alloys. Metall Mater Trans A 36A:657–666. https://doi.org/10.1007/s11661-005-0099-y
10. Cavaliere P (2018) Cold-spray coatings recent trends and future perspectives. Springer, Cham
11. Romero JE, Byers WA, Wang G, et al (2017) Simulated severe accident testing for evaluation of accident tolerant fuel. 2017 Water react. Fuel Perform Meet
12. Shah H, Romero J, Xu P et al (2017) Development of surface coatings for enhanced accident tolerant fuel. 2017 Water react. Fuel Perform Meet
13. Lee C, Kim J (2015) Microstructure of kinetic spray coatings: a review. J Therm Spray Technol 24:592–610. https://doi.org/10.1007/s11666-015-0223-5
14. Sansoucy E, Marcoux P, Ajdelsztajn L, Jodoin B (2008) Properties of SiC-reinforced aluminum alloy coatings produced by the cold gas dynamic spraying process. Surf Coat Technol 202:3988–3996. https://doi.org/10.1016/j.surfcoat.2008.02.017
15. Fernandez R, Jodoin B (2017) Effect of particle morphology on cold spray deposition of chromium carbide-nickel chromium cermet powders. J Therm Spray Technol 26:1356–1380. https://doi.org/10.1007/s11666-017-0580-3

16. Wolfe DE, Eden TJ, Potter JK, Jaroh AP (2006) Investigation and characterization of Cr3C2-based wear-resistant coatings applied by the cold spray process. J Therm Spray Technol 15:400–412. https://doi.org/10.1361/105996306X124400
17. Al-Mangour B, Mongrain R, Irissou E, Yue S (2013) Improving the strength and corrosion resistance of 316L stainless steel for biomedical applications using cold spray. Surf Coat Technol 216:297–307. https://doi.org/10.1016/j.surfcoat.2012.11.061
18. Smith WH, Seybolt AU (1956) Ductile chromium. J Electrochem Soc 103:347. https://doi.org/10.1149/1.2430326
19. (1990) Properties of pure metals: ASM handbook, Vol.2. ASM International
20. Sova A, Grigoriev S, Okunkova A, Smurov I (2013) Potential of cold gas dynamic spray as additive manufacturing technology. Int J Adv Manuf Technol 69:2269–2278. https://doi.org/10.1007/s00170-013-5166-8
21. Yeom H, Maier BR, Johnson G, Sridharan K (2018) Cold spray coatings for accident tolerant Zr-alloy cladding in light water reactors. In: Trans. Am. Nucl. Soc. American Nuclear Society, Philadelphia, PA USA, pp 1576–1579
22. Allen RF (1999) Standard test methods for determining average grain size (F112). https://doi.org/10.1520/E1382-97R04
23. Choi IC, Brandl C, Schwaiger R (2017) Thermally activated dislocation plasticity in body-centered cubic chromium studied by high-temperature nanoindentation. Acta Mater 140:107–115. https://doi.org/10.1016/j.actamat.2017.08.026
24. Maier V, Hohenwarter A, Pippan R, Kiener D (2015) Thermally activated deformation processes in body-centered cubic Cr—how microstructure influences strain-rate sensitivity. Scr Mater 106:42–45. https://doi.org/10.1016/j.scriptamat.2015.05.001
25. King PC, Zahiri SH, Jahedi M (2009) Microstructural refinement within a cold-sprayed copper particle. Metall Mater Trans A 40:2115–2123. https://doi.org/10.1007/s11661-009-9882-5
26. Luo XT, Li CX, Shang FL, Yang GJ, Wang YY, Li CJ (2014) High velocity impact induced microstructure evolution during deposition of cold spray coatings: a review. Surf Coat Technol 254:11–20. https://doi.org/10.1016/j.surfcoat.2014.06.006
27. Furukawa M, Horita Z, Nemoto M, Valiev RZ, Langdon TG (1996) Microhardness measurements and the hall-petch relationship in an Al-Mg alloy with submicrometer grain size. Acta Mater 44:4619–4629. https://doi.org/10.1016/1359-6454(96)00105-X
28. Brittain CP, Armstrong RW, Smith GC (1985) Hall-petch dependence for ultrafine grain size electrodeposited chromium. Scr Metall 19:89–91. https://doi.org/10.1016/0036-9748(85)90271-6
29. Yuuji K, Setsuo T (1995) Microstructural changes during annealing of work-hardened mechanically milled metallic powders (overview). Mater Trans JIM 36:289–296. https://doi.org/10.2320/matertrans1989.36.289
30. Al-Mangour B, Vo P, Mongrain R et al (2014) Effect of heat treatment on the microstructure and mechanical properties of stainless steel 316L coatings produced by cold spray for biomedical applications. J Therm Spray Technol 23:641–652. https://doi.org/10.1007/s11666-013-0053-2
31. Li CJ, Li WY, Wang YY (2005) Formation of metastable phases in cold-sprayed soft metallic deposit. Surf Coat Technol 198:469–473. https://doi.org/10.1016/j.surfcoat.2004.10.063
32. Zhang P, Li SX, Zhang ZF (2011) General relationship between strength and hardness. Mater Sci Eng A 529:62–73. https://doi.org/10.1016/j.msea.2011.08.061
33. Chen C, Xie Y, Huang R, Deng S, Ren Z, Liao H (2018) On the role of oxide film's cleaning effect into the metallurgical bonding during cold spray. Mater Lett 210:199–202. https://doi.org/10.1016/j.matlet.2017.09.024
34. Li WY, Zhang C, Wang HT, Guo XP, Liao HL, Li CJ, Coddet C (2007) Significant influences of metal reactivity and oxide films at particle surfaces on coating microstructure in cold spraying. Appl Surf Sci 253:3557–3562. https://doi.org/10.1016/j.apsusc.2006.07.063